Hydride Transfer to Gold: Yes or No? Exploring the Unexpected Versatility of Au···H-M Bonding in Heterobimetallic Dihydrides

Luca Rocchigiani,[a]* Wim T. Klooster,[b] Simon J. Coles,[b] David L. Hughes,[a] Peter Hrobárik,[c]* and Manfred Bochmann [a]*

[a] School of Chemistry, University of East Anglia, Norwich Research Park, Norwich, NR47TJ, United Kingdom - Email: L.Rocchigiani@uea.ac.uk, M.Bochmann@uea.ac.uk

[b] National Crystallography Service, School of Chemistry, University of Southampton, Southampton SO171BJ, United Kingdom

[c] Department of Inorganic Chemistry, Faculty of Natural Sciences, Comenius University, SK-84215 Bratislava, Slovakia - Email: peter.hrobarik@uniba.sk

Abstract

The potential for coordination and H-transfer from Cp_2MH_2 (M = Zr, W) to gold(I) and gold(III) complexes was explored in a combined experimental and computational study. $[(L)Au]^+$ cations react with Cp_2WH_2 giving $[(L)Au(\kappa^2\text{-}H_2WCp_2)]^+$ (L = IPr (**1**), cyclic (alkyl)(amino)carbene (**2**), or phosphines PPh_3 (**3**) and Dalphos-Me (**4**) [IPr = 1,3-bis(di*iso*propylphenyl)imidazolylidene; Dalphos-Me = di(1-adamantyl)-2-(dimethylamino)phenyl-phosphine], while $[Au(DMAP)_2]^+$ (DMAP = *p*-dimethylaminopyridine) affords the C_2-symmetric $[Au(\kappa\text{-}H_2WCp_2)_2]^+$ (**5**). The Dalphos complex **4** can be protonated to give the bicationic adduct **4H**, showing Au(I)···H^+-N hydrogen bonding. The gold(III) Lewis acid $[(C\text{^}N\text{-}CH)Au(C_6F_5)(OEt_2)]^+$ binds Cp_2WH_2 to give an Au-H-W σ-complex. By contrast, the pincer species $[(C\text{^}N\text{^}C)Au]^+$ adds Cp_2WH_2 by a purely dative W→Au bond, without Au···H interaction. The biphenyl-based chelate $[(C\text{^}C)Au]^+$ forms $[(C\text{^}C)Au(\mu\text{-}H)_2WCp_2]^+$, with two 2-electron-3-centre W-H···Au interactions and practically no Au-W donor acceptor contribution. In all these complexes strong but polarised W-H bonds are maintained, without H-transfer to gold. On the other hand, the reactions of Cp_2ZrH_2 with gold complexes led in all cases to rapid H-transfer and formation of gold hydrides. Relativistic DFT calculations were used to rationalize the striking reactivity and bonding differences in these heterobimetallic hydride complexes along with an analysis of their characteristic NMR parameters and UV-Vis absorption properties.

Introduction

Gold-based catalysts[1] have attracted much attention over the past two decades and proved to be very active in promoting a large family of reactions with potential industrial interest. Heterogeneous gold catalysts are efficiently used in hydrogenation,[2] hydrosilylation,[3] acetylene hydrochlorination[4] and water-gas shift reactions.[5] Likewise, homogeneous gold complexes find applications in hydrogenation and hydrosilylation catalysis.[6,7] H_2 activation and hydrogen transfer reactions are key steps in these catalytic cycles. Several mechanistic studies suggested the formation of gold hydrides as reaction intermediates, both in homogeneous[8] and heterogeneous[9,10,11] processes, but details about their mode of action remain limited.

Recent years have seen significant advances in the chemistry of molecular gold hydrides, both for Au(I)[12] and Au(III).[13,14] For example, we have shown that detectable σ-complexes of silanes and boranes are formed as intermediates to H-transfer to gold,[13d,15] which occurs heterolytically in the presence of a basic solvent leading to stable Au(III) hydrides. Similarly, H_2 and even C-H bonds of activated hydrocarbons proved to be susceptible to heterolytic cleavage.[13d]

On the other hand, the reactivity of well-defined gold hydride complexes in catalysis does not necessarily match that of heterogeneous systems. In heterogeneous catalysis the interchange of H-atoms from one metal to another or between a metal and a support is of course well-known; indeed it is fundamental to our understanding of the operation of multicomponent heterometallic catalysts and metal-support effects.[16] For example, hydrogen spillover is being discussed in the context of Fischer-Tropsch catalysis by Au-promoted Co catalysts,[17] in the reaction of H_2 with Au/Pt assemblies,[18] in the electrocatalytic hydrogen evolution reaction on Pt/Au films,[19] in small Au_xTi_y clusters on hydroxylated silica,[20] and in Au/TiO_2 catalysts.[21] Gold-metal interactions are also an intrinsic part of the intermetallic electronic communication in supported bimetallic nano-catalysts.[22] At a molecular level, several types of interactions may be envisaged for hydrogen transfer from a substrate or an H-carrying support to the metal centre of a catalyst, such as structures **I** – **V** (Scheme 1).

The aim of the present study is to provide information about the possible bonding that might occur during hydrogen transfer to gold. This requires a judicious choice of the H-E substrate, which should be able to act as H donor and at the same time allow the isolation of potentially informative intermediates. Such a substrate would also need to possess an electron pair, i.e. Lewis basicity, to resemble the chemistry of H-E moieties such as surface-OH groups. We identified Cp_2WH_2 as a suitable candidate, as it is basic like N or O donors and, at the same time, it can function as hydride source. In interactions with other metals it may act simply as a lone-pair donor, form σ-H

complexes, or form bridging hydrides involving 2-electron-3-centre (2e3c) type bonding, as illustrated in structures **A** – **G**. It remains unclear, however, which of these bonding motives can be found in Au(I/III) systems, and which factors lead to their formation.

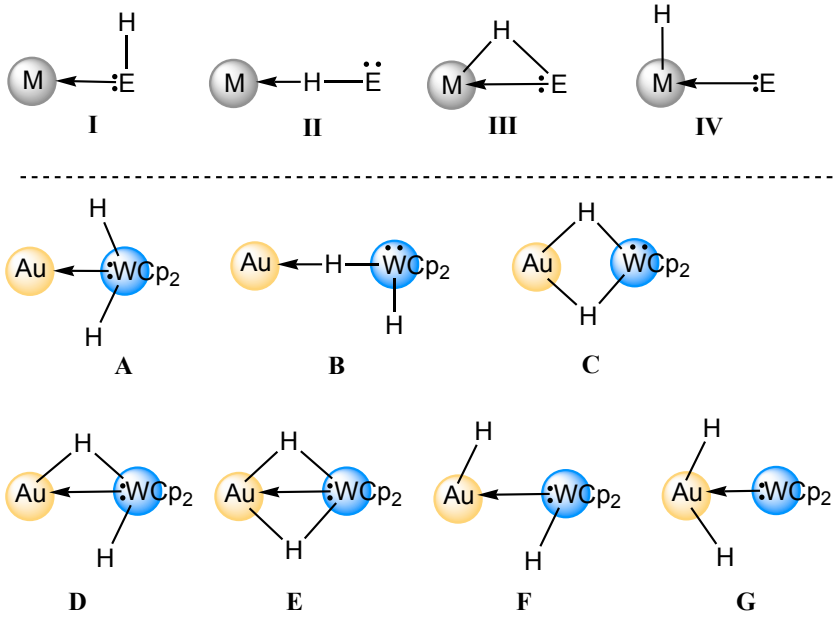

Scheme 1. Top: Illustrative interactions **I** – **IV** between a metal centre M and heteroatom H-E moieties leading to hydrogen spill-over. Bottom: Potential interaction modes **A** – **G** between gold centres and Cp_2WH_2.

Heterobinuclear H-bridged complexes involving gold are of course not without precedent. In pioneering work in the 1980s, Stone *et al*. reported the synthesis of the neutral $[Ph_3PAu(\mu\text{–}H)M(CO)_5]$ complexes, where M = Cr, Mo and W,[23] while Venanzi isolated the cationic complexes $[Ph_3PAu(\mu\text{–}H)Ir(H)_2PPh_3][BF_4]$ and $[Et_3PAu(\mu\text{–}H)Pt(PEt_3)_2(C_6Cl_5)][BF_4]$.[24] These species have been described as donor-acceptor complexes, where the cationic phosphine gold(I) fragment accepts electron density from the hydride, establishing a 2-electron-3-centre bond, with an additional contribution of a metal-metal interaction that explains the remarkable stability of these complexes. This strategy has been extended to other transition metals such as Nb,[25] Ru,[26] Os.[27] More recent studies revealed that these species might turn into interesting catalytic systems; for example, Crimmin reported that heterobimetallic copper-gold hydrides can hydroborate CO_2 in the presence of pinacolborane in high selectivity to give formate derivatives.[28]

From a mechanistic point of view, Au–H–M moieties can be seen as a situation where the hydride transfer is arrested in an intermediate stage.[29] One of the aspects that seems key for the stabilization of gold heterobimetallic hydrides is the ability of gold to interact with the second metal and form a donor-acceptor complex. The reactivity of transition metal hydrides towards a gold

cation is therefore expected to differ according to the d-electron count and the hydricity of the M-H species involved. To test this, the reactivity of well-defined cationic Au(I) and Au(III) species with Cp_2WH_2 was compared with that of Cp_2ZrH_2; these metal dihydrides possess closely comparable M–H bond energies (bond dissociation enthalpies: $Cp^*_2ZrH_2$ 339 kJ/mol; Cp_2WH_2 311±4 kJ/mol) but different electron configurations.[30] Both metallocene dihydrides are known to form heterometallic compounds with bridging hydride interactions: Cp_2ZrH_2 gives stable adducts with Mg, Zn and Al hydrides,[31] while Cp_2WH_2 has been extensively explored in combination with many cationic late metal centers, including Al, [32] Rh,[33] Pt[34] and rare earth metals.[35] Cp_2WH_2 is also a good ligand for isolated Cu and Ag centers,[36] while to our knowledge there is no precedent for W-Au dihydrides.

We demonstrate here that the fundamental difference between Zr and W[37] determines the fate of gold heterobimetallic hydrides. While Cp_2ZrH_2 undergoes very rapid hydride transfer reactions, stable heterobimetallic hydride-bridged gold-tungsten adducts can be obtained and characterized both for Au(I) and Au(III) by using ligand configurations of types **H** – **K** (Scheme 2). A surprisingly varied range of interactions was found, including W→Au donor/acceptor bonds, σ-complexes, and 3c2e bonding with and without additional metal-metal bonding contribution. The structure and bonding has been elucidated with the help of NMR spectroscopy, X-ray and neutron diffraction, as well as relativistic DFT calculations, which revealed the importance of Coulomb contribution to bonding and H-transfer.

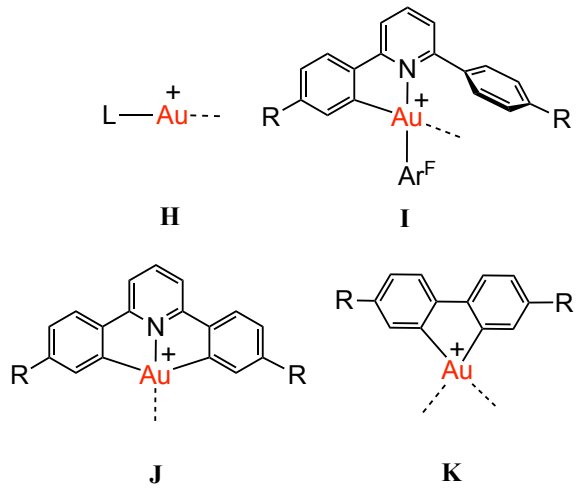

Scheme 2. Generic structures of gold(I, III) complexes used in the present study: R=*tert*-butyl.

Results and Discussion

Gold(I) complexes

The reactivity of different cationic gold(I) complexes with Cp_2WH_2 has been explored using the acetonitrile adducts [LAu(NCMe)][SbF_6] (Scheme 3).[38] As proved by NMR spectroscopy,

[LAu(NCMe)][SbF_6] and $CpWH_2$ react instantaneously in CD_2Cl_2 at 297K to afford the adducts [LAu(μ-H)$_2$WCp_2)][SbF_6] **1** – **4** quantitatively, without any trace of reduction. Analytically pure samples of **1** – **4** were obtained in good yields from larger-scale reactions and further recrystallization from CH_2Cl_2 / light petroleum.

The reaction of bis-(4-dimethylaminopyridine)gold(I) triflate with 2 molar equivalents of Cp_2WH_2 in CH_2Cl_2 affords the homoleptic complex **5**, which was obtained as an analytically pure microcrystalline solid after washing with hexane/toluene and recrystallization from CH_2Cl_2/light petroleum. The heteroleptic intermediate $Cp_2W(\mu–H)_2Au(DMAP)^+$ could not be isolated.

The complete multinuclear NMR characterization of complexes **1** - **5** revealed that the ^{1}H NMR signals of the hydride and the ^{13}C NMR resonances of the cyclopentadienyl ligands are high-frequency shifted with respect to Cp_2WH_2. The hydride NMR signals of **1** – **5** become more positive in the order δ_H(**1**) ≈ δ_H(**2**) < δ_H(**3**) = δ_H(**4**) < δ_H(**5**) (cf. Table 1). The values of the $^1J_{183W-H}$ coupling constant decrease only slightly in the series, ranging from 72.0 (**1**) to 66.0 Hz (**5**), and are in good agreement with those computed using relativistic quantum-chemical calculations (see DFT section below). The carbene-carbon atoms in **1** and **2** resonate at δ_C = 201.3 and δ_C = 256.8 ppm, respectively. These values are very similar to analogous neutral IPr[39] and ^{Ad}CAAC[40] complexes featuring strong electron-donor carbon-based ligands. The NMR data for all new complexes in comparison with computed NMR parameters are given Table 1.

A systematic inspection of DFT optimized and X-ray determined Au–C and Au–N bond-lengths in *trans*-[LAu(IPr)]^q and *trans*-[LAu(C^N^C)]^q series, respectively, revealed that Cp_2WH_2 bound to the Au(I) center exerts a weaker *trans* influence than the hydride (H^-) ligand alone, comparable rather with the *trans* influence of sulphides or CO, while Cp_2WH_2 coordinated to the Au(III) center via W→Au dative bonding (see discussion below) has one of the strongest *trans* influences, comparable with silyl or boryl ligands (cf. Tables S13 and S14 in SI).

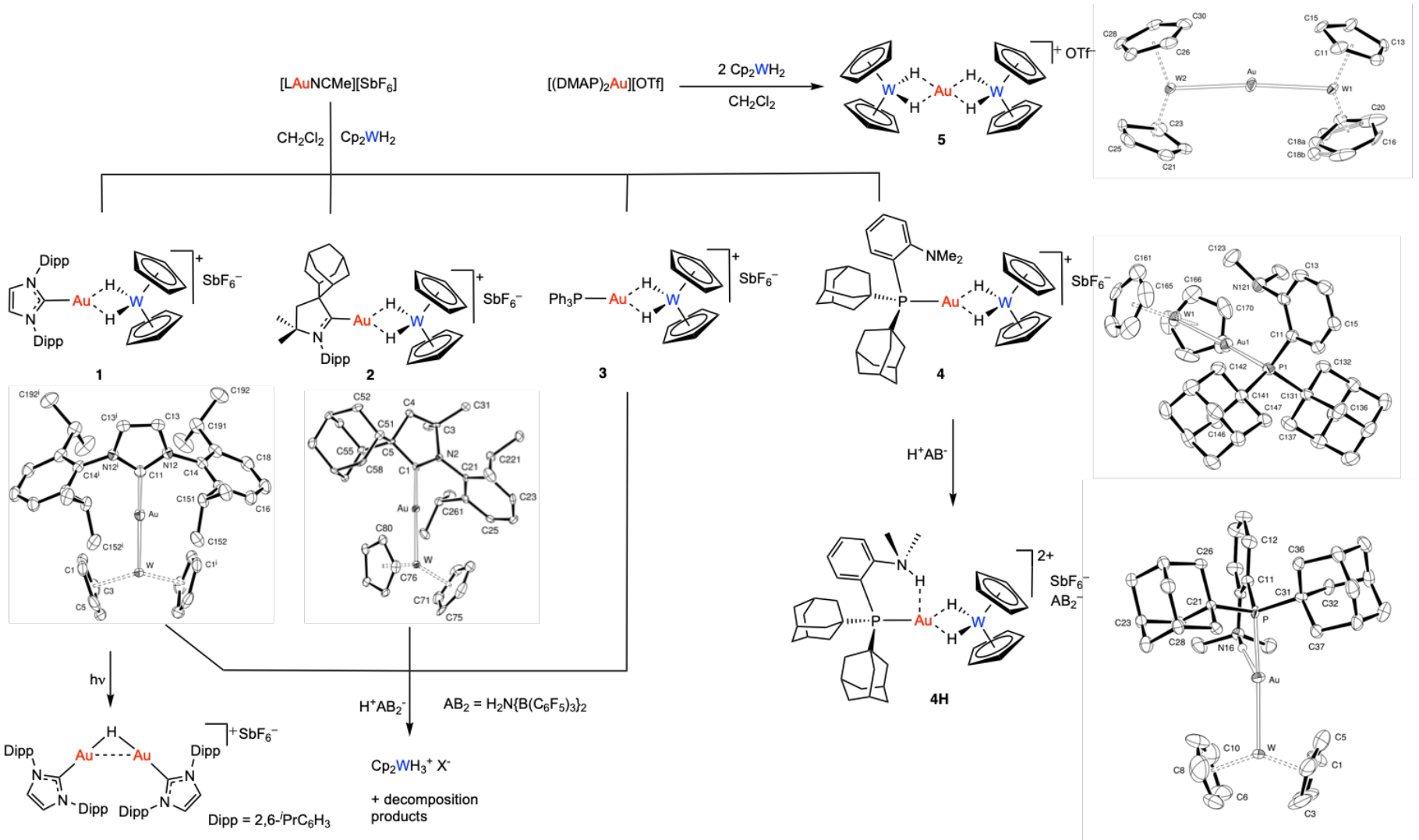

Scheme 3. Synthesis of Au(I)/W(IV) dihydrido complexes **1**-**5** (dipp = 2,6 di-*iso*propylphenyl; DMAP=4-dimethylaminopyridine), X-ray structures of **1**, **2**, **4**, **4H** and **5**. Thermal ellipsoids are set at 50%, H atoms, anion and solvent are omitted for clarity. The hydride ligands were not located. Selected bond distances (Å) and angles (°): **1**: Au–W 2.7394(5), Au–C11 1.994(9), C11–Au–W 177.5(3), $Cp_{centroid}$–W–$Cp_{centroid}$ 144.37. **2**: Au-W 2.7600(4), Au–C1 2.013(6), C1–Au–W 175.63(17), $Cp_{centroid}$–W–$Cp_{centroid}$ 144.37. **4**: Au1–W1 2.7587(4), Au1–P1 2.2753(17), P1–Au1–W1 177.43, $Cp_{centroid}$–W–$Cp_{centroid}$ 146.18. **5**: Au–W1 2.7784(7), Au–W2 2.7686(7), W2–Au–W1 171.61(3), Cp–W2–Cp 140.71, Cp–W1–Cp 142.97.

The structures of **1**, **2**, **4** and **5** were confirmed by single-crystal X-Ray diffraction (Scheme 3). In all the cases, the L–Au–W core is almost linear. The position of the hydrides could not be located and refined due to the large electron density of the two metal centres. The molecular structures all show very similar geometric parameters. The Au–W distances vary only slightly in the order **1** (2.7394(5) Å) > **4** (2.7587(4) Å) ≈ **2** (2.7600(4) Å) > **5** ($d_{Au–W1}$ = 2.7784(7), $d_{Au–W2}$ = Å 2.7686(7) Å), with no apparent correlation with either δ_H or $^1J_{WH}$. The interaction between the two metal centers induces only a moderate decrease of the $Cp_{centroid}–W–Cp_{centroid}$ angle α between the two cyclopentadienyl ligands of the Cp_2W unit with respect to free Cp_2WH_2 (α = 150.53°), with Δα values of about –6.2° (**1** and **2**), –4.3° (**4**) and –9.8° (**5**).

In the carbene complexes **1** and **2** the plane described by the two Cp centroids and the tungsten atom is essentially coplanar with the carbene scaffold. In the phosphine complex **4** the hydride ligands are oriented towards the dimethylamino group, and the $Cp(centroid)_2W$ plane is about perpendicular to the 2-aminophenyl. In the W-Au-W complex **5** the two Cp_2W units are eclipsed (dihedral angle Cp1–W1–W2–Cp3 ~7.5°). This suggests that the four hydrides describe a square-planar like environment around the gold atom, similar to the previously reported $[\{Cp''_2NbH(\mu–H)_2\}_2Au]^+$ cation (Cp″ = 1,3-$C_5H_3(SiMe_3)_2$).[25] However, computational results show that a C_2 structure, in which only one of the two H ligands in Cp_2WH_2 is tightly bonded to the gold centre, represents the minimum structure, although the energy differences are small (*vide infra*). A near-tetrahedral coordination geometry is realized in the silver analogue, $[Cp_2W(\mu–H)_2]_2Ag$, [36b] where the Cp1–W1–W2–Cp3 dihedral angle is much larger (49.5°). Complex **5** also shows the largest deviation from linearity (W–Au–W 171.61°), similar to the analogous silver complex (170.77°).

Complex **1** afforded crystals large enough for a neutron diffraction experiment, which has been used to determine the exact position of the hydrides in the complex (Figure 1). The Au-H bond lengths in the AuH_2W core are moderately different, 1.96(4) Å and 2.12(4) Å (Δd = 0.16 Å) while the two W–H distances are coincident (W–H1: 1.72(4) Å, W–H2: 1.72(5) Å); see the DFT discussion below.

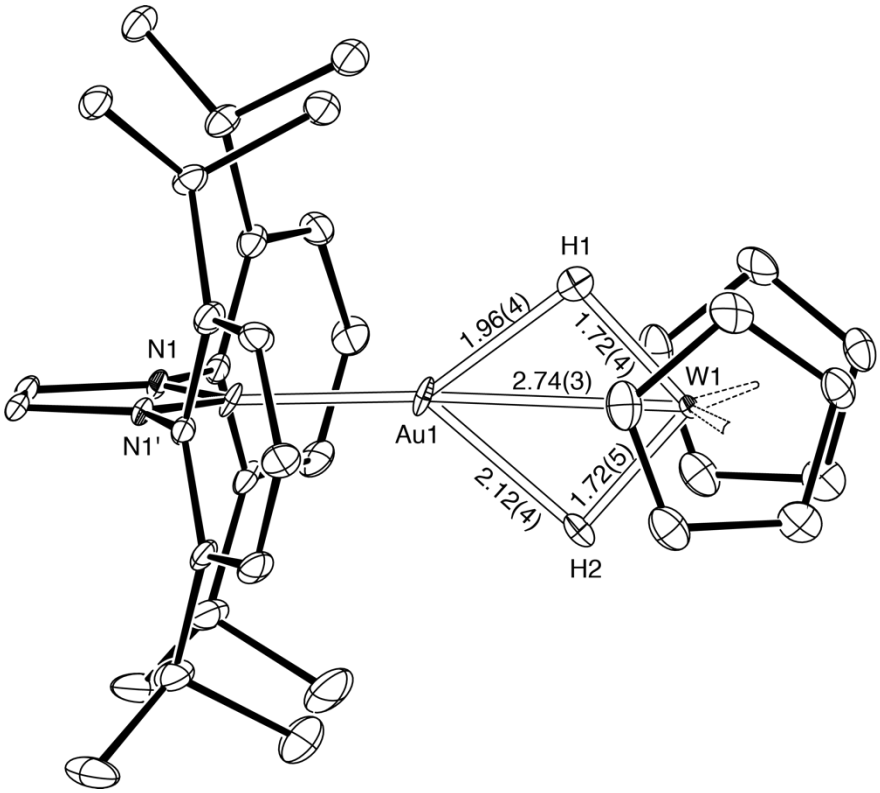

Figure 1. Molecular structure of **1** derived from neutron diffraction experiments. Thermal ellipsoids are set at 50%, anion and solvent are omitted for clarity. Bond distances are in Å.

Under anaerobic and dark conditions complexes **1** - **5** are thermally stable in THF solution for an indefinite amount of time at room temperature; however, they are photolyzed by UV light. Irradiating the carbene complex **1** at 365 nm for 48h in [D_8]THF induces a clean conversion to the known homobimetallic hydride [(IPrAu)$_2$(μ–H)][SbF_6] (Scheme 3), suggesting that a single hydride is transferred from tungsten to gold and no reductive elimination of H_2 takes place. This is supported by the observation of a tungstenocene monohydride species (δ_H = -12.5 ppm) at early stages of the reaction. However, the latter is not stable and decomposes after prolonged exposure to UV light. UV photolysis was also observed for **2** and **3**, but no clean product could be isolated as extensive reductive decomposition occurred.

Coordination of Cp_2WH_2 to gold is easily reversible. For example, **1** reacts instantaneously with 1 equivalent of tris-*p*-tolyl phosphine affording [(IPr)Au(Ptol_3)][SbF_6] and 1 equivalent of free Cp_2WH_2. Treatment of **1** – **3** with strong acids, such as [$H(OEt_2)_2$][$H_2N\{B(C_6F_5)_3\}_2$], affords [Cp_2WH_3]$^+$ [$H_2N\{B(C_6F_5)_3\}_2$]$^-$ together with gold decomposition products. By contrast, in the reaction of **4** with 1 equivalent of [$H(OEt_2)_2$][$H_2N\{B(C_6F_5)_3\}_2$] the Au–W unit is preserved and instead the bicationic ammonium complex **4H** is formed (Scheme 3), as suggested by the appearance of a broad singlet at δ_H = 11.5 ppm and the splitting of the NMe_2 signal into a doublet

($^3J_{HH}$ = 4.9 Hz). The NMR features of the hydride signal (δ_H = –9.2 ppm, $^1J_{WH}$ = 71.8, $^2J_{PH}$ = 21.0 Hz) are close to those of the precursor complex **4**.

Single crystals of **4H** were obtained from CD_2Cl_2/light petroleum. Upon crystallization, anion reorganization occurred and large crystals of **4H** featuring two amido-diborate anions were obtained. The geometric parameters of **4H** are closely similar to those of **4**. The Au–W distance (2.7616(7) Å) is practically unaltered, while elongations of the P–Au (2.360(2) Å) and Au–N distances (3.126 Å) are observed. The amino H-atom was not observed but was included in an approximately tetrahedral site; this H atom is 2.15 Å from the Au centre and the N-H-Au angle is 174.1 °.

The structure of **4H** is interesting for two reasons. Firstly, an acidic N-H proton is located in immediate proximity to hydride ligands, without H-H coupling and H_2 elimination. Secondly, the interaction of gold centres with polar NH moieties has recently been the subject of experimental and theoretical studies on the existence of H···Au hydrogen bonding, where it was shown that energetically significant NH···Au interactions may exist for Au(I)[41] but not for Au(III).[42] In this regard, DFT calculations for **4H** revealed an extremely short Au(I)···H^+(N) contact (2.114 Å, see Scheme 3) connected with somewhat higher covalency (DI(Au···H) = 0.164) as compared with recently reported cases[41] and show that an active Au···H^+ hydrogen bonding can be present also between two positively charged fragments/units (note that DI stands for a QTAIM delocalization index, which integrates the electron density in the region between two atoms in question and serves thus as a measure of the bond-covalency). Similarly with recent reports, this is reflected in a high-frequency shift of the ^{1}H NMR signal of the dimethylammonium group and large spin-orbit (SO)-induced shielding of the $^{15}NHMe_2$ nitrogen (σ^{SO} = 6.2 ppm), which arises from a heavy Au(I) center mediated through the Fermi contact mechanism via the Au(I)···H^+–N interaction. We note further that this interaction is also seen in the NBO analysis as a coupling between the occupied "lone-pair" orbital on gold and antibonding σ*(N-H) with stabilization energy $E^{(2)}$ of -13.4 kcal.mol^{-1}.

By contrast to the formation of thermally stable gold adducts of Cp_2WH_2, the reaction of Au(I) with Cp_2ZrH_2 leads to instantaneous hydride transfer, without any detectable H-bridged intermediates. For example, treatment of [(IPr)Au(NCMe)][SbF_6] with Cp_2ZrH_2 generated [$(IPr)_2Au_2(\mu–H)$][SbF_6],[12a] while with [(PPh_3)Au(NCMe)][SbF_6] and [$Au(DMAP)_2$][OTf] fast reduction to Au(0) was observed (Scheme 4).

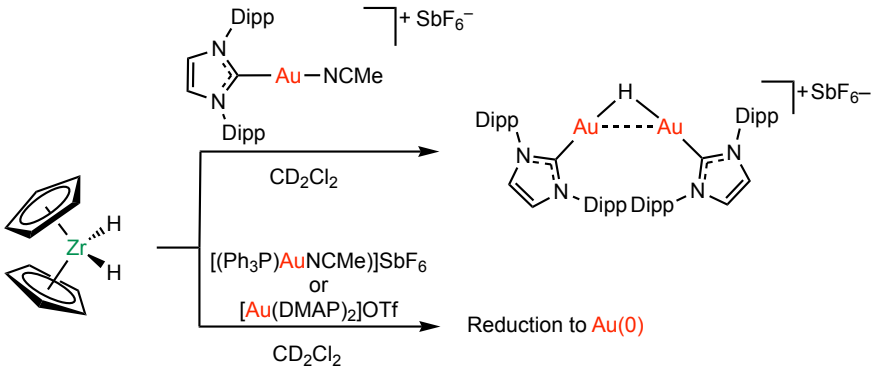

Scheme 4. Reaction of Au(I) complexes with Cp_2ZrH_2 (dipp = 2,6-^{i}Pr$_2$C$_6$H$_3$).

Gold(III) complexes

Cyclometalated ligands offer a very efficient platform for the stabilization of labile Au(III) intermediates and reactivity studies.[43,44] Here we use complexes based on cyclometalated C^C, C^N and C^N^C ligands to probe the reactivity of high-valent gold with Cp_2MH_2 (M = Zr, W), in order to assess the role of oxidation state and ligand geometry on the Au(III)–H–W interaction mode.

(i) σ-Complexes

The Lewis acidic C^N chelate complex $[(C^N–CH)Au(C_6F_5)(OEt_2)]^+AB_2^-$ [AB_2 = H_2N-$\{B(C_6F_5)_3\}_2$][45] reacts with 1 equivalent of Cp_2WH_2 at –50 °C in CD_2Cl_2 to give a deep-red solution. The ^{1}H NMR spectrum shows the presence of two separate hydride signals at δ_H = -9.63 and δ_H = -11.40 ppm, which were assigned to the adduct **6** (85% yield), together with the signals for the Au(I) compound **5** and the $[Cp_2WH_3]^+$ cation (triplet at δ_H = -6.10 and doublet at δ_H = -6.46) (Scheme 5). Complex **6** is thermally unstable and can only be studied at –50 °C. The presence of two distinct hydride signals in the ^{1}H NMR spectrum suggests that only one of the two H ligands in Cp_2WH_2 is bound to gold, forming a σ-complex. At this temperature interchange of the H ligands in **6** is slow on the NMR time scale, although the ^{1}H NOESY NMR spectrum shows that the complex is fluxional, as terminal and bridging hydrides are in chemical exchange. The difference between the two hydrides is also reflected in the $^1J(^{183}W–H)$ coupling constants, which decrease from 61.0 Hz for the bridging hydride (δ_H = –9.63 ppm) to 48.0 Hz for the terminal W-H (δ_H = –11.40 ppm). The σ-coordination of one H-W bond in **6** resembles the bonding situation observed generally in Au-H-E complexes (E = B, Si[13d] or C[15]).

Cp_2WH_2 is found to exert a strong *trans*-influence, as judged by the ^{13}C NMR shift of the cyclometalated carbon atom (δ_C = 170.0 ppm), which is comparable to the terminal hydride in $(C^N–CH)Au(C_6F_5)H$ (δ_C = 170.5 ppm) and much higher than the ^{13}C resonances in the bridging

hydride [{(C^N–CH)Au(C_6F_5)}$_2$(μ–H)]$^+$ (δ_C = 159.5 ppm)[13c] and in the silane complex [(C^N–CH)Au(C_6F_5)(HSiEt$_3$)]$^+$ (δ_C = 150.6 ppm).[13d]

The formation of the [Cp_2WH_3]$^+$ cation is likely due to oxidation of Cp_2WH_2 by traces of [$H(OEt_2)_2$][H_2N{$B(C_6F_5)_3$}$_2$]. The formation of the gold(I) complex **5** as a by-product suggests that Cp_2WH_2 also triggers reduction to Au(I) with C-C bond formation of the C_6F_5 and C^N ligands, in a manner seen before in reductive eliminations induced by SMe_2.[46] Warming the sample to above –20 °C allows the reductive elimination to go to completion within 30 minutes. This reaction probably follows a stepwise mechanism (Scheme 5)[45] and leaves **5** as the only hydride-containing product in about 50% yield, along with an intractable black solid.

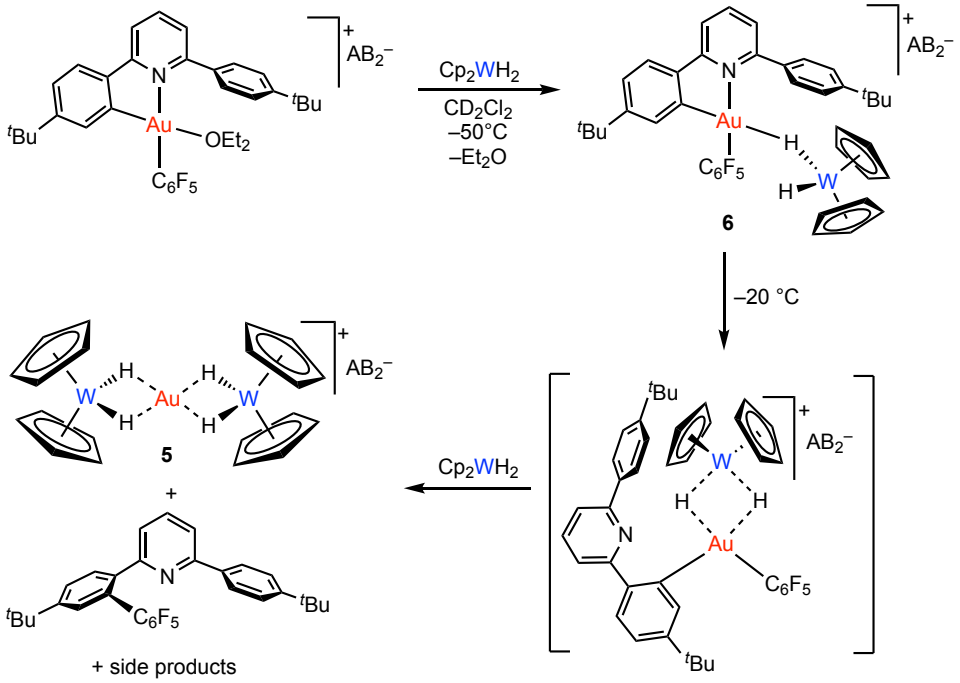

Scheme 5. Reactivity of [(C^N–CH)Au(C_6F_5)(OEt_2)]$^+$ with Cp_2WH_2. (AB_2 = H_2N{$B(C_6F_5)_3$}$_2$).

(ii) Au-W donor-acceptor bonding

A completely different scenario is observed when 1 molar equivalent of Cp_2WH_2 is reacted at -50 °C with the *in situ* generated species [(C^N^C)Au][$Ac^FOB(C_6F_5)_3$] (Scheme 6). Both ^{1}H and ^{19}F NMR spectra of the reaction mixture obtained soon after mixing revealed that tungsten dihydride displaces the anion from the first coordination sphere and generates an ionic complex **7**. The two Cp rings and the hydrides give rise one ^{1}H NMR singlet each. The hydride signal is remarkably high-frequency shifted with respect to free Cp_2WH_2 and resonates at δ_H = –3.33 ppm, with a $^1J(^{183}W–H)$ coupling constant of 38.0 Hz. These low values are unusual for a Cp_2WH_2-based fragment and are more similar to the chemical shifts of W(VI) polyhydrides, such as $Cp_2WH_3^+$ or $CpWH_5(PMe_3)$. This observation suggests that a significant modification of the electronic properties of the tungsten

atom occurs upon interaction with gold. However, the NMR fingerprint of the (C^N^C)Au fragment showed little change, suggesting that no redox reaction had taken place. Unfortunately, **7** proved thermally unstable and decomposes above –20 °C with H-transfer to the C^N^C ligand (Scheme 6) and a crystal structure could not be obtained. With the help of DFT calculations (*vide infra*) we suggest that **7** is a Lewis adduct of Au(III), with a W→Au dative bond but without gold-hydrogen interactions.

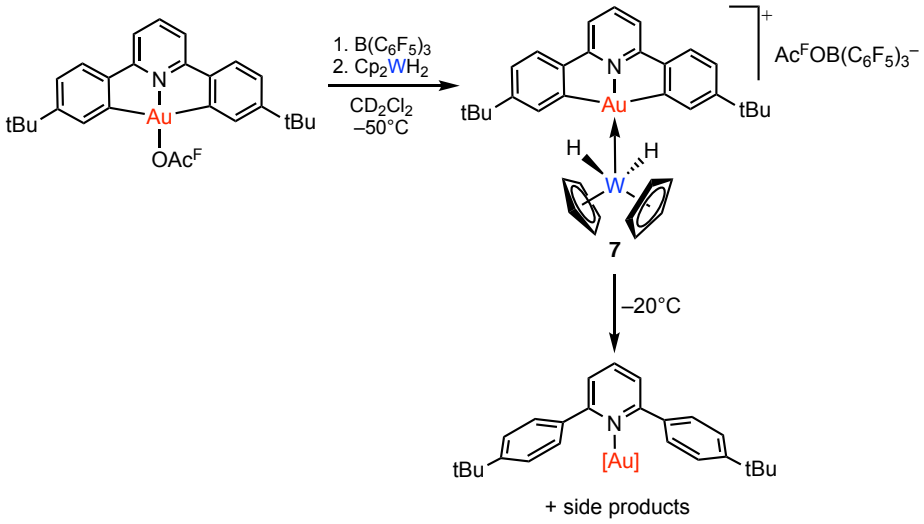

Scheme 6. Reactivity of [(C^N^C)Au^{F}AcOB(C_6F_5)] with Cp_2WH_2; [Au] = Au^+ or $AuOAc^F$.

(iii) 2-electron-3-centre bonded complexes

In contrast with the previous cases, the reaction of the C^C chelate complex $[(C^C)Au(COD)]^+$ (C^C = 4,4′-di-*t*-butylbiphenyl-2,2′-diyl, COD = 1,5-cyclooctadiene)[47] with 1 molar equivalent of Cp_2WH_2 in CH_2Cl_2 gave the thermally stable adduct **8**, which can be obtained as a pure material after evaporation of cyclooctadiene (Scheme 7). Solutions of **8** in CH_2Cl_2 are characterized by a very distinctive lilac colour (absorption centred at λ = 540 nm), which is in contrast to other (C^C)Au(III) derivatives which are typically pale-yellow. The hydride ^{1}H NMR signal in **8** (δ_H = –11.48 ppm) is only moderately high-frequency shifted with respect to free Cp_2WH_2 and is quite similar to the Au(I) adducts **1** and **2**. However, the $^1J(^{183}W–H)$ coupling constant is considerably higher (92.4 Hz), suggesting a different bonding situation. Since the $[(C^C)Au]^+$ cation has two orbitals of the correct symmetry for forming Au-H σ-bonds, as in the $[(C^C)AuH_2]^-$ anion,[13c] but no LUMO along the Au-W vector suitable for a donor interaction with the d^2-W centre, the Au-H interaction in **8** consists of two Au-H-W 2e-3c bonds without direct metal-metal interaction. The two hydride ligands exert a large *trans* influence on the ^{13}C NMR chemical shift of the gold-bound C-atoms, which resonate at δ_C = 177.2 ppm (DFT computed δ_C

shift: 178.2 ppm). This is quite similar to the value observed for terminal hydrides of the type (C^C)AuH(L).

When an excess of Cp_2WH_2 is used, the hydride signal of **8** broadens at room temperature, indicating exchange of Cp_2WH_2. This is confirmed by ^1H NOESY NMR experiments performed at -50 °C. Evidently the coordination of Cp_2WH_2 to gold is labile and a second tungsten can displace the bridging hydride moiety.

Single crystals of **8** suitable for X-Ray diffraction were obtained from a CH_2Cl_2 solution layered with toluene. Although the position of the hydrides could not be determined, the molecular structure (Scheme 7) confirmed the identity of the complex suggested by NMR spectroscopy. The tungstenocene unit is slightly tilted away from the plane described by the two aryl rings, with a $Centroid_{C22/C21}$–Au–W angle of 170°. This orientation places both the hydrides in the ideal position for interacting with the acceptor sites of Au(III) in the typical square-planar configuration. This bonding differs substantially from the situation found for the Au(I) adducts, where a distortion of the L–Au–W bond is always very similar (139.65° vs. 140.23°), suggesting that both the hydrogen atoms of Cp_2WH_2 interact with the gold centre. Consistent with this, Au–C bond distances of the C^C ligand are elongated (Au–C11 = 2.027 Å, Au–C20 = 2.046 Å) due to the strong *trans* influence exerted by the hydride donors.

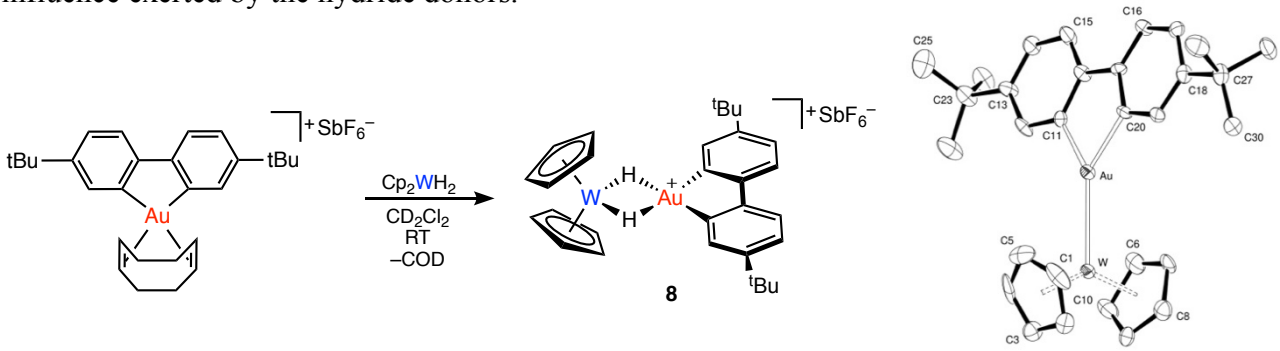

Scheme 7. Synthesis and molecular structure of **8**. Thermal ellipsoids are set at 50%, anion and solvent are omitted for clarity. Selected bond distances (Å) and angles (°): Au–W 2.7034(7), Au–C11 2.027(13), Au–C20 2.047(12), C11–Au–W 139.6(4), C20–Au–W 140.2(4), $Cp_{centroid}$–W–$Cp_{centroid}$ 140.25.

(iv) H-transfer reactions

In analogy with the results obtained with Au(I) precursors (Scheme 4), the reactions of Cp_2ZrH_2 with Au(III) complexes do not afford heterobimetallic adducts but give fast and quantitative hydride transfer to gold. Even at –50 °C the ether adduct [(C^N–CH)Au(C_6F_5)-(OEt_2)][AB_2] instantly cleaves the Zr–H bond of Cp_2ZrH_2, to give the bridging hydride [{(C^N–CH)Au(C_6F_5)}$_2$(μ–H)][AB_2]. The zirconium by-product is [$Cp_2ZrH(OEt_2)$][AB_2]. The same

products were found using the ether-free cation [(C^N–CH)AuC$_6$F$_5$][AB$_2$], which suggests that the presence of ether is not required to trigger heterolytic Zr-H bond cleavage.

In the reaction of zirconocene dihydride with the pincer complex [(C^N^C)Au][Ac^{F}O-B(C$_6$F$_5$)$_3$] at –50 °C, the Au(III) hydride (C^N^C)AuH was observed in 40% conversion, as suggested by the appearance of the typical ^{1}H NMR signal at δ_H = –6.5 ppm.[13a] This reaction was accompanied by the formation of extensive side products, due to the fragmentation of the trifluoroacetate borate anion upon reaction with zirconium hydrides.

Even more striking is the reaction of Cp$_2$ZrH$_2$ with the biphenyl complex [(C^C)Au(COD)]$^+$. No transient gold hydride was observed. Even at –78 °C a black precipitate was formed, and the ^{1}H NMR spectrum at –50 °C revealed the formation of free biphenyl ligand (50% yield by NMR) as the product of reductive C-H elimination (Scheme 8).

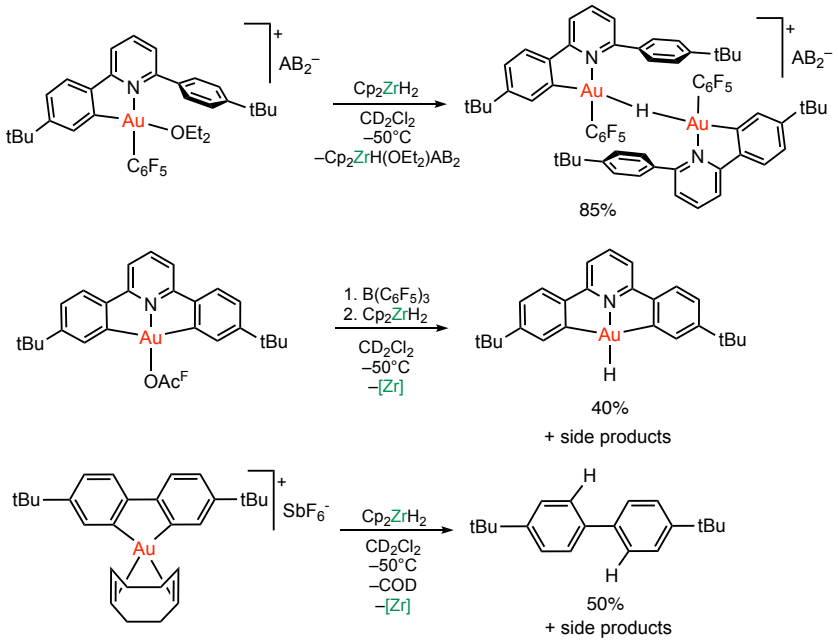

Scheme 8. Reactions of Au(III) chelate complexes with Cp$_2$ZrH$_2$; conversion obtained by NMR *in situ*.

DFT Calculations

Since not all bimetallic adducts were characterized by X-ray crystallography and positions of hydrides could not be refined precisely in the metal environment, we utilized relativistic DFT calculations to elucidate all structures systematically and to compute characteristic NMR parameters (hydride shifts and corresponding *J* couplings with neighbouring atoms) to confirm the presence of bimetallic hydrides along with their specific interactions also in solution. Besides we

wanted to shed more light on the bonding situation in these bimetallic hydride species and to rationalize some of the striking differences observed above.

All investigated structures were optimized at the PBE0-D3(BJ)/ECP/def2-QZVP level using a quasi-relativistic small-core pseudopotentials for tungsten and gold, along with atom-pairwise corrections for dispersion forces (see Figures 2 and 3 for the calculated structures of the gold(I) and gold(III) complexes, respectively, and Table 2 for pertinent bond-lengths). First, we note a good agreement between X-ray and DFT optimized structures, with differences in W···Au and Au−L distances often less than 0.03 Å, with the exception of complex **4** with somewhat longer W···Au contact (by 0.049 Å) computed at the DFT level. Optimized W-H bond-lengths in **1** are in good match with those from elastic neutron scattering measurements (W-H_{av} : 1.722 Å vs. 1.738 Å) and two Au···H interactions exhibit a notable asymmetry (shorter and longer Au···H contact), although this is more pronounced in the DFT optimized structure (Table 2). The averaged Au···H distances are 2.101 Å and 2.036 Å in DFT and neutron diffraction structures, respectively. The modest deviation between experimental and computed Au···H bond-lengths can be attributed to crystal packing effects in the solid-state and lack of genuine covalent Au-H bonds (see below), resulting in a shallow barrier to hydride interchange.

The analysis confirms that in the Au(I) complexes **1** – **5** the interaction between Cp_2WH_2 and the gold(I) fragments involves almost exclusively the hydride bridge, without a significant additional W···Au donor-acceptor interaction; the contribution of gold orbitals to the W···Au interaction is less than 5%. Within the W-H-Au core the W-H bond remains strong, while the contribution of the gold-H interaction is small, with an orbital contribution of the order of only 3-5 %. Coordination of Cp_2WH_2 therefore leads neither to hydride transfer, nor to the formation of covalent Au-H bonds. Given the lack of covalent Au-H bonds, there is only a shallow barrier to H-interchange, and the complexes are fluxional.

The fluxionality of Au···H interactions is best demonstrated in $[(Cp_2WH_2)Au(H_2WCp_2)]^+$ (**5**), where three saddle points with C_2, D_{2h} and C_{2v} symmetries were found (Figure 2). All three conformers lie energetically close to each other. The global minimum is the C_2 structure, with a distorted square-planar environment around the gold atom and two asymmetric Au···H bonding modes (two shorter and two longer Au···H contacts with bond-lengths of 1.823 and 2.330 Å), while tetrahedral D_{2h} ($d_{Au\cdots H}$ = 1.987 Å) and planar C_{2v} ($d_{Au\cdots H}$ = 1.976 Å) structures with four virtually equivalent Au···H interactions are energetically disfavoured by 0.3 and 1.9 kcal.mol^{-1}, respectively (Figure 2b). The unusual arrangement of Cp_2WH_2 ligands in the C_2 isomer of **5** maximizes both the electrostatic and orbital (covalent) interactions (cf. Table S3 in SI). We note that this is in striking contrast with lighter group 11 (Cu and Ag) analogues of **5**, which were found to feature a

pseudotetrahedral coordination of hydrides around the metal center in the solid-state, that is in accordance with our DFT calculations (cf. SI, Tables S2 and S3). The tendency of Au(I) to form asymmetric (shorter and longer) Au···H contacts in most of W···Au dihydrides (**1** - **4**) and polyhydrides (**5**) can be attributed to its general preference for a linear two-coordinate geometry, resulting from the diminished energy gap between the 6s, 6p and 5d orbitals due to relativistic effects. By contrast, lighter analogues prefer the formation of three- and four-coordinated complexes.[48]

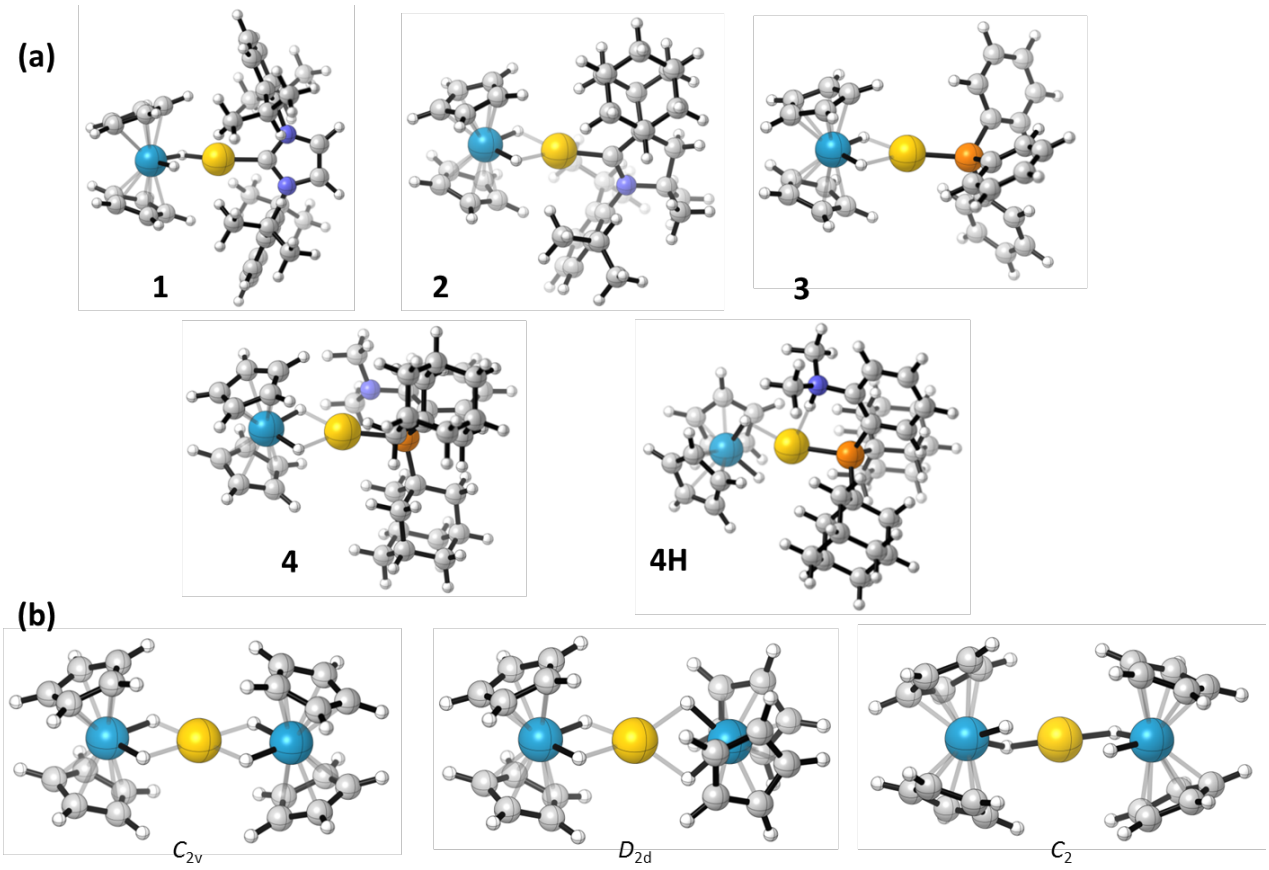

Figure 2. (a) Calculated structures of complexes **1** – **4** and the Au···HN bonded complex **4H**, showing the asymmetry of Au-H interactions. Pertinent interatomic distances and comparisons with X-ray data are given in Table 2. (b) Diagrams of the C_{2v}, D_{2h} and C_2 saddle points of complex **5**. The C_2 structure represents the global minimum.

Table 1. Experimental and computed hydride ^{1}H NMR characteristics in Cp_2WH_2, $Cp_2WH_3^+$ and bimetallic adducts of Cp_2WH_2 with various Au(I/III) species (**1**-**8**) [a,b]

		Experimental		Calculated			
Complex		$\delta(^1H)$ [ppm]	$^1J(^{183}W,^1H)$ [Hz]	$\delta(^1H)$ [ppm]	$\delta(^1H)$ [ppm]	$\delta(^1H)_{av}$ [ppm]	$^1J(^{183}W,^1H)$ [Hz]
Cp_2WH_2		-13.1	73.7	-13.1	-13.1	-13.1	76.8
$Cp_2WH_3^+$		-6.4[d]	47.0	-6.4[d]	-6.1[e]		51.8[d]
		-5.8[e]	68.0				79.2[e]
$[(Cp_2WH_2)Au(IPr)]^+$	**1**	-11.0	72.0	-11.1	-10.7	-10.9	75.2
$[(Cp_2WH_2)Au(CAAC)]^+$	**2**	-10.7	72.5	-10.7	-10.2	-10.5	75.7
$[(Cp_2WH_2)Au(PPh_3)]^+$	**3**	-9.4	71.0	-8.4	-8.4	-8.4	76.3
$[(Cp_2WH_2)Au(Dalphos\text{-}Me)]^+$	**4**	-9.4	69.0	-9.5	-9.3	-9.4	71.1
$[(Cp_2WH_2)AuH(Dalphos\text{-}Me)]^{2+}$	**4H**	-9.2	71.8	-9.5	-8.4	-9.0	73.9
$[(Cp_2WH_2)Au(H_2WCp_2)]^+$	**5**	-8.4	66.0	-10.1	-7.8	-9.0	69.0
$[(Cp_2WH_2)Au(C\text{^}N\text{–}CH)(C_6F_5)]^+$	**6**	-9.6[f]	61.0[f]	-9.1[f]	-12.0[g]		61.9[f]
		-11.4[g]	48.0[g]				50.5[g]
$[(Cp_2WH_2)Au(C\text{^}N\text{^}C)]^+$	**7**	-3.3	38.0	-3.5	-3.2	-3.3	37.6
$[(Cp_2WH_2)Au(bph\text{-}^tBu)]^+$	**8**	-11.5	92.4	-12.3	-12.3	-12.3	90.2

[a] Chemical shifts calculated at the 2c-ZORA(SO)/PBE0-XC/TZ2P level using a COSMO solvation model (CH_2Cl_2 as the solvent; cf. Computational details). [b] Nuclear spin-spin couplings calculated at the 2c-ZORA(SO)/PBE0-50HF/TZ2P/COSMO(CH_2Cl_2) level (cf. Computational details). [c] Au-H hydrogen bonding. [d] Lateral WH_2 hydride atoms. [e] Central WH hydride atom. [f] Bridging W-H hydride atom bound to Au. [g] Terminal W-H hydride atom non-bound to Au.

Table 2. Pertinent contacts in DFT optimized structures of Cp_2MH_2 (M = W, Zr) and bimetallic adducts of Cp_2MH_2 with various Au(I/III) species[a]

		DFT optimized distances [Å]											X-ray [Å] [b]
Complex		M···Au	M-H	M-H	M-H_{av}	Au···H	Au···H	Au···H_{av}[c]	Au···H[d]	Au-C	Au-P	Au-N	W···Au
Cp_2WH_2			1.709	1.709	1.709								
$(Cp_2WH_2)Au(IPr)^+$	**1**	2.762	1.703	1.747	1.725	1.861	2.341	210.1		200.8			2.739
$(Cp_2WH_2)Au(CAAC)^+$	**2**	2.780	1.720	1.738	1.729	1.927	2.130	202.9		201.6			2.760
$(Cp_2WH_2)Au(PPh_3)^+$	**3**	2.733	1.716	1.717	1.717	2.121	2.130	212.6			2.278		–
$(Cp_2WH_2)Au(Dalphos\text{-}Me)^+$	**4**	2.808	1.722	1.743	1.733	1.967	2.049	200.8			2.293		2.759
$(Cp_2WH_2)AuH(Dalphos\text{-}Me)^{+2}$	**4H**	2.744	1.707	1.736	1.722	2.030	2.253	207.2	211.4		2.333		2.750
$(Cp_2WH_2)Au(H_2WCp_2)^+$	**5**	2.797	1.705	1.777	1.741	1.823	2.330	207.7					2.774
$(Cp_2WH_2)Au(C\text{^}N\text{-}CH)(C_6F_5)^+$	**6**	3.064	1.676[e]	1.760[f]		1.859[f]	2.958[e]			2.005[g]		2.119	–
										2.039[h]			–
$(Cp_2WH_2)Au(C\text{^}N\text{^}C)^+$	**7**	2.802	1.657	1.660	1.658	2.434	247.6	245.5		2.110[i]		2.063	–
$(Cp_2WH_2)Au(bph\text{-}^tBu)^+$	**8**	2.720	1.793	1.793	1.793	1.884	188.4	188.4		2.022[i]			2.703
Cp_2ZrH_2			1.877	1.877	1.877								
$(Cp_2ZrH_2)Au(IPr)^+$		2.830	1.829[e]	2.137[f]	1.983	1.641[f]	335.8[e]						
$(Cp_2ZrH_2)Au(bph\text{-}^tBu)^+$		2.892	2.024	2.026	2.025	1.733	173.3	173.3		2.032[i]			

[a] Optimizations done at the PBE0-D3(BJ)/def2-QZVP/COSMO level. [b] W···Au distance determined by X-ray. [c] The averaged Au···H distance of Au···H_2MCp_2 interactions. [d] Au···H(N) hydrogen bonding. [e] Hydride atom with no interaction to Au. [f] Bridging hydride atom. [g] Au-C_{C6F5}. [h] Au-$C_{C\text{^}N\text{-}CH}$. [i] The averaged Au–C distance.

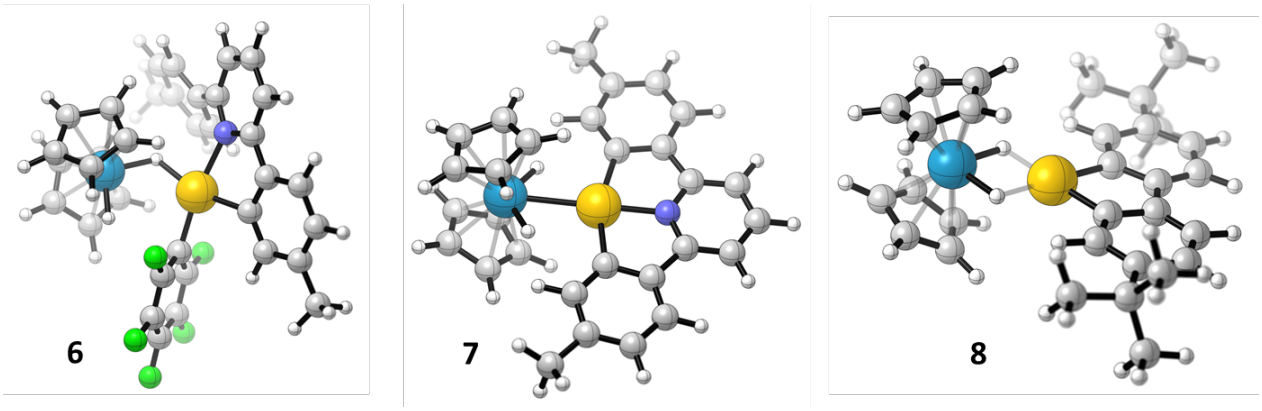

Figure 3. Calculated structures of complexes **6** – **8**, exemplifying a σ-complex (**6**), a W→Au donor interaction (**7**), and a 2e3c-hydride bridged system lacking a W→Au interaction (**8**). See Table 2 for pertinent interatomic distances.

The reliability of DFT-determined structures, including W−H and Au−H bond-lengths, is further demonstrated by the excellent agreement between computed and experimental ^{1}H hydride NMR shifts, with a standard deviation of 0.5 ppm, as well as corresponding nuclear spin-spin couplings with hydride ligands, with a standard deviation of 2.2 Hz for $^{1}J(^{183}W,^{1}H)$ constants (see Table 1 and ESI, Tables S5, S6 and Figures S1 and S2). The NMR parameters were obtained at the two-component ZORA-SO level, including spin−orbit coupling. Interestingly, the spin-orbit contribution to hydride shifts is relatively small across the entire series **1** - **8** ($|\sigma^{SO}|< 1.5$ ppm) and apart from bridging hydrides in **6** and **8** it has a shielding character. This along with large paramagnetic shielding contributions suggests a stronger W-H bond covalency in comparison with the Au···H interaction (the former being however weakened in comparison with the W-H bond in parent Cp_2WH_2) and thus none of the adducts **1** - **8** can be considered as a true gold hydride. Modest changes in ^{1}H hydride shifts of bimetallic adducts **1** - **8** are caused by all three components (diamagnetic, paramagnetic and spin-orbit), σ^{SO} being however minor.

The hydride shift of **7** (δ_H = -3.3 ppm) is notably deshielded when compared to the other adducts within the series (with δ_H ranging from -11.5 to -8.4 ppm). This might be attributed to the different bonding in **7**. This complex has the strongest W(d^2)→Au dative interaction (see NLMO analysis in Table S9 and discussion below); this pushes the W($5d^2$) electrons to gold (although the W-Au bond is still polarized towards tungsten), reduces the Buckingham-Stephens off-centre ring currents (experienced as an effective diamagnetic/diatropic current at the position of W-H hydride ligands) and leads to the notably smaller paramagnetic shielding (σ^p). Complex **7** therefore shows the most covalent W-Au bond, while W-H···Au interactions are virtually absent (see below). These characteristics are also reflected in the shortest W-H bonds (1.658 Å) and in the smallest $^{1}J(^{183}$W-H) coupling (38.0 Hz).

The bonding in **7** is in sharp contrast with **8**, which shows the largest $^{1}J(^{183}W\text{-}H)$ value (92.4 Hz) and the longest W-H bonds (1.793 Å; see also Tables S1, S5 and S6 in SI). We note, however, that the correlation between $^{1}J(^{183}W\text{-}H)$ coupling constants and W-H distances is only rough within the investigated series (R^2 = 0.668; see Figure S25 in SI), which is understandable taking into account the different coordination modes of the hydrides (bridging vs. terminal) and the different oxidation states of gold. Whereas we have shown previously that it is possible to estimate the Au-H bond lengths in homometallic gold hydrides from their ^{1}H NMR chemical shifts,[13c] in the present case such a correlation cannot be used for a reliable estimation of W-H bond lengths from measured NMR parameters.

To get deeper insight into bonding and electronic structure of adducts **1** - **8**, we performed energy decomposition analysis (EDA) of $LM^{+}\cdots H_2M'Cp_2$ interactions (M = Cu, Ag, Au; M' = W, Zr) as well as bond analysis using quantum-theory-of-atoms-in-molecules (QTAIM), natural bond orbitals (NBO), natural localized molecular orbitals (NLMO) and electron localization function (ELF). EDA analysis revealed that the interaction energy (ΔE_{int}) between Cp_2WH_2 and LAu^{+} fragments ranges from -67.5 kcal/mol (**4**) to -113.1 kcal/mol (**7**) and it is dominated by electrostatics (54-65%). The covalent orbital contribution (ΔE_{orb}) varies from -62.2 kcal/mol (**4**) up to -100.2 kcal/mol (**7**) and corresponds to 30-40% of all attractive interactions (electrostatic, orbital and dispersion, with dispersion forces contributing only about 3-8%). Interestingly, although no clear trends can be established between ΔE_{int} and salient bond-lengths and/or NMR spectroscopic parameters, the thermal stability of bimetallic adducts **1**-**8** seem to be related to the covalency percentage ($\%\Delta E_{orb} = \Delta E_{orb}/(\Delta E_{orb}+\Delta E_{elstat}+\Delta E_{disp})$) estimated from EDA. Specifically, the most labile adducts feature the highest $LAu^{+}\cdots H_2WCp_2$ covalency ($\%\Delta E_{orb}$ above 35%). This finding can be rationalized by the fact that more covalent interactions between LAu^{+} and H_2WCp_2 fragments lead to strengthening of Au-H and/or Au-W bonds, which in turn polarize the W-H bonds and trigger thus decomposition pathways of the relatively inert Cp_2WH_2 ligand (including its oxidation and/or hydride transfer).

This is also apparent when comparing the thermally stable adduct $[(C\text{^}C)AuH_2WCp_2]^{+}$ (**8**) with its putative zirconium congener. The latter features higher interaction energy and orbital covalency between LAu^{+} and metallocene dihydride fragments as compared to **8** (see SI, Table S4). The increased Zr-H bond ionicity in Cp_2ZrH_2 and its putative adducts with Au(I)/Au(III) species (see NPA charges in Table S8 and QTAIM delocalization indices, as a measure of bond covalency/ionicity, in Table S11) facilitates hydride transfer reactions and makes decomposition pathways energetically preferable. Scheme 9 illustrates these trends for the case of complex **7** and its zirconium analogue. Cp_2WH_2 is somewhat more reluctant to hydride transfer due to higher W-H

bond covalency as compared to Cp_2ZrH_2, but since the energy difference between adduct formation and hydride transfer is often small (note that both processes are strongly exoenergetic), the increased temperature or applied UV light induces the decomposition of adducts.

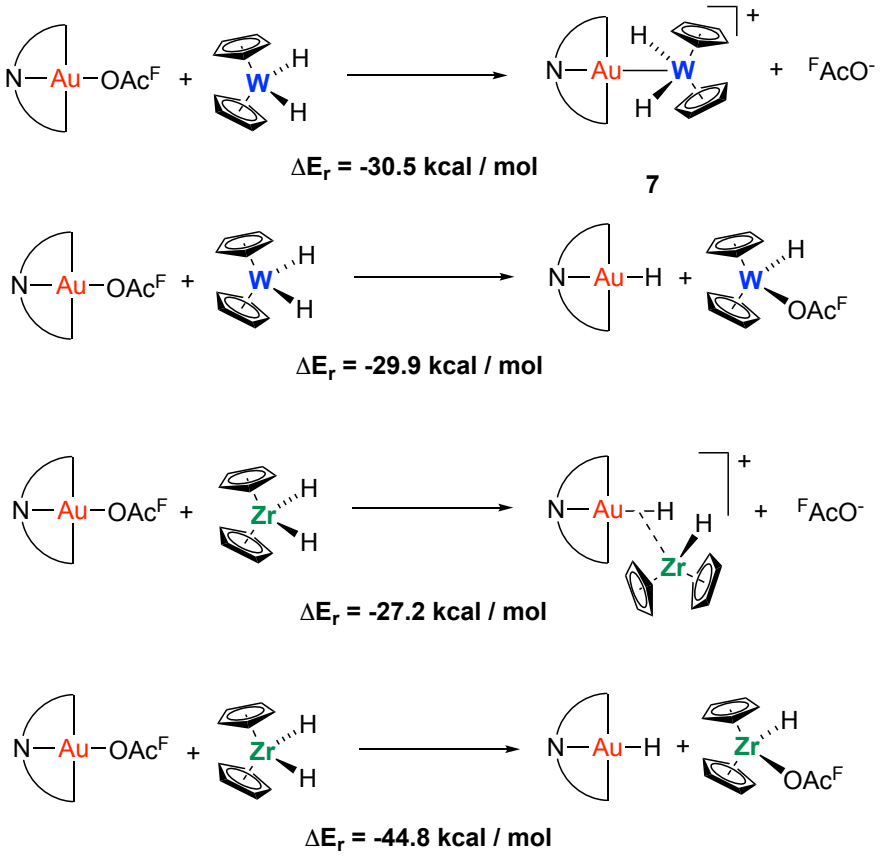

Scheme 9. Computed reaction energies for the reaction of (C^N^C)AuOAc^F with metallocene dihydrides (PBE0-D3(BJ)/ECP/def2-QZVP results), illustrating the preferential formation of an Au-M adduct if M = W and H-transfer if M = Zr.

From an orbital point of view, bonding between LAu^+ and Cp_2WH_2 can be ascribed to the donor-acceptor interactions between σ(W-H) occupied MOs and the vacant, predominantly Au-centred MOs with a significant 6s/5d character as well as to the interaction of the latter vacant orbitals with an occupied W($5d^2$) MO. According to NBO second-order perturbation energy analysis, the adducts are mostly stabilized by the σ(W-H)→σ*(Au-L) interactions, which are seen in NLMO (and in related adaptive natural density partitioning, AdNDP, analysis) as three-center two-electron (3c2e) bonds (see Figure S27 in SI). These are strongly polarized towards W-H with a small, variable contribution of gold (3-7% for bridging W-H···Au interactions), the latter participating mostly through Au(6s) orbital in the case of Au(I) adducts or via both Au(6s) and Au(5d) in the case of Au(III) adducts. Dative W($5d^2$)→σ*(Au-L) interactions contribute

energetically by ca. 15-30% as compared to the bridging W-H···Au bond (cf. Table S10 in SI). The weaker donation from W(d^2) as compared to that from hydride ligands might be attributed to the small positive charge at tungsten centre (Table S8) and to an interaction of the occupied W($5d_{xy}$) orbital with two cyclopentadienyl rings, as inspected from NLMO and AdNDP analysis of parent Cp_2WH_2 and its adducts (see SI, Figure S26). Interestingly, replacement of the Cp rings in some of the investigated complexes with Cl ligands led to structures with notably shorter W···Au distances (by ~0.1-0.2 Å).

A bonding analysis of **7** and **8** illustrates the two extremes of Au(III)-H_2WCp_2 interactions. The formation of the thermally labile adduct **7** is driven by the strongest dative W→Au interaction within the series, which is also seen in the composition of corresponding NLMO orbital – the W-Au bond in **7** involves 34.5% of gold (26% Au(6s), 74% Au(5d)), while in all other cases the gold percentage contribution in the W···Au bonding is at the level 0.5-4.5%, except that in **8** dative interactions are practically absent (cf. Figure S26 in SI). The different bonding situations in **7** and **8** are also seen in ELF plots (Figure 4), which show a clear bonding attractor between two metal centres in **7** and its absence in **8**.

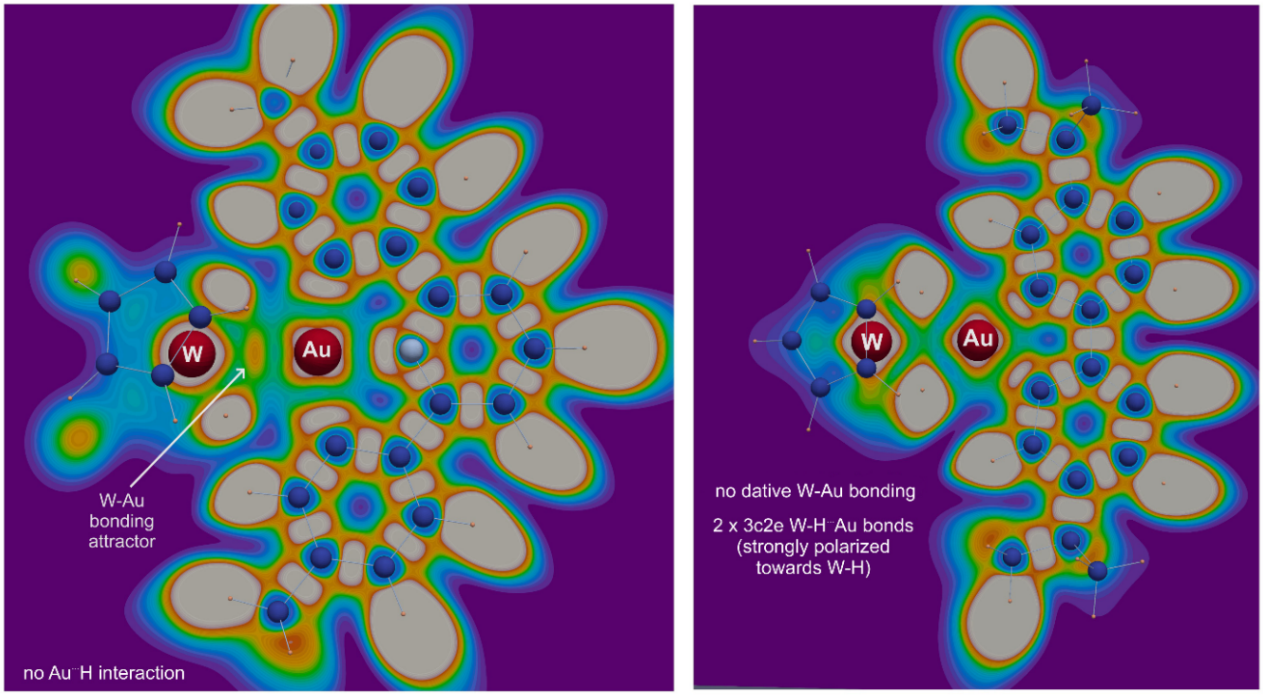

$[(Cp_2WH_2)Au(C^N^C)]^+$ (**7**) $[(Cp_2WH_2)Au(bph)]^+$ (**8**)

Figure 4. Cut-plane plots from ELF analysis of bonding in adducts **7** (left) and **8** (right). The gray-white and orange regions represent ELF maxima (bonding attractors). The selected planes go through the tungsten, gold and two hydride atoms.

Hence, it is obvious that electrostatics along with orbital σ(W-H)→σ*(Au-L) interactions (without any W···Au dative bonding) are strong enough to stabilize most of the bimetallic hydrides investigated herein, but the bonding is quite fluxional, as found in our ^{1}H NMR experiments. Coordination of Cp_2WH_2 to Au(I)/Au(III) therefore leads at ambient conditions neither to hydride transfer, nor to the formation of covalent Au-H bonds. Interestingly, the extent of W-H bond polarisation and Au-H bond formation in Au(I) complexes with Cp_2WH_2 (**1** - **5**) is in striking contrast with the electronic structure computed for a previously characterized gold-tungsten hydride, $[(Ph_3P)Au(\mu\text{-}H)W(CO)_5]$ (**9**)[23a] (cf. Figure S28 in ESI for comparison of relevant diagnostics in structurally related PPh_3 complexes **3** and **9**). Unlike **3**, complex **9** features a remarkably shorter Au-H contact (1.707 Å) than the W···H interaction (1.920 Å), that is associated with higher (lower) Au-H (W-H) bond covalency (DI(Au-H) = 0.681; DI(W-H) = 0.392) and reflected in notably different hydride NMR characteristics (expt.: δ_H = -2.45 ppm; $^{1}J_{183W,H}$ = 44 Hz; $^{2}J_{31P,H}$ = 107 Hz; DFT calcd.: δ_H = -2.60 ppm; $^{1}J_{183W,H}$ = 46 Hz; $^{2}J_{31P,H}$ = 104 Hz) as compared to **3**.

One aspect that remains to be explored is the reason for the (for gold) unusual lilac color of **8**. The excitation energies calculated at the time-dependent DFT level (PBE0/ECP/def2-TZVP/PCM) for some of the bimetallic hydrides **1** - **8** match the experimental observations (cf. Table S12 and Figure S6). While Au(I) adducts (**1** - **5**) and Au(III) complex **7** are computed to feature absorptions in the (near) ultraviolet region (300–390 nm) and should thus be colorless or light yellow, complexes **6** and **8** exhibit the lowest-lying absorption bands in the visible region at 490 nm and 539 nm, respectively, corresponding to their red and purple colors (the vis absorption band measured for **8** was found at 540 nm; see Figure S18 in ESI for UV-vis absorption spectra). The lowest-lying excitations correspond to electron transitions from HOMO (**1**-**7**) or HOMO-1 (**8**) to LUMO (Table S12). Apart from **7**, the former occupied MOs have largely a W(5d) character, while vacant LUMOs are mostly centered at Au and adjacent ligand atoms (in some cases also with the W(5d) contribution; cf. Figure S29). Hence, the lowest energy excitations in **1**-**6** and **8** can be viewed as charge-transfers from Cp_2WH_2 unit to AuL fragment (Cp_2WH_2→AuL), as also confirmed by NPA charge analysis of the ground and first excited states. While LUMOs in Au(I) complexes feature relatively high energies (~-1.3 to -1.5 eV) and Au(I) species absorb thus in the UV region, the LUMOs in Au(III) species are notably stabilized – the more so the larger Au(5d) admixture – shifting the absorption to the visible spectral region (with the lowest LUMO level found in **8**). In contrast, dative W→Au bonding in **7** stabilizes the occupied W(d^2) orbital to such extent that it becomes HOMO-5 (instead of being HOMO or HOMO-1 as in all other cases), increasing thus the energy gap with LUMO. As a consequence, the lowest-lying absorption in **7** can

be viewed as electron transition within the AuL fragment alone rather than the charge-transfer $Cp_2WH_2 \rightarrow AuL$.

Conclusions.

Investigating the interactions of metallocene dihydrides with gold(I) and gold(III) complexes has revealed a surprisingly varied range of bonding and reaction types. Whereas in the case of the d^0 metallocene Cp_2ZrH_2 transfer of hydride to gold takes place in all cases, the analogous d^2 system Cp_2WH_2 forms a variety of adducts with diverse Au···H-M bonding motives, which may also exist in parallel (*e.g.* hydride-bridged W–H···Au interactions and Au···$^+$HN hydrogen bonding in bicationic gold(I) complex, **4H**). With Au(I) centres Cp_2WH_2 acts as donor ligand, mainly via σ(W-H)→σ*(Au-L) interactions. The contribution due to W→Au donor interactions is smaller, and the complexes are fluxional. For the $[Au(H_2WCp_2)_2]^+$ cation a structure with asymmetric Au-H contacts and a two-coordinate H-Au-H core is energetically slightly preferred.

In gold(III) complexes all three of the potential coordination types **A**, **B** and **C** in Scheme 1 are realised, and in the σ-complex $[(C\hat{}N–CH)Au(C_6F_5)(\mu\text{-}H)WHCp_2]^+$ (**6**) the hydride-interchange is slow on the NMR time scale. The only case where a significant W→Au donor-acceptor interaction is realised, without Au···H bonding contributions, is the adduct of the pincer cation $[(C\hat{}N\hat{}C)Au]^+$, while the complex with $[(C\hat{}C)Au]^+$ realizes the opposite extreme, a complex relying exclusively on two 2-electron-3-centre Au-H-W bonds since energetically accessible orbitals of the suitable symmetry required for a W···Au interaction are absent. In all these hydride complexes, the W-H bond is polarised but remains present, while true covalent Au-H bonds are not yet formed. This is surprising, given the general strength and covalent character of Au-H bonds in isolable gold hydride complexes, and differs from the reactions of gold(III) centres with borane, silane and hydrocarbon H-E bonds. The increase in polarity of hydrides like W-H may however provide bonding insight into the increased reactivity of supported gold catalysts in hydrogenation reactions, where such interactions may be envisaged to take place in the gold-support boundary layer.

Keywords: bridging ligands – density functional calculations – gold – hydrides – tungsten

Acknowledgement.

This work was supported by the European Research Council. MB is an ERC Advanced Investigator Award holder (grant no. 338944-GOCAT). Calculations were performed using the supercomputing infrastructure acquired in projects ITMS 26230120002 and 26210120002 supported by the Research & Development Operational Programme funded by the ERDF. PH also acknowledges

financial support from the Slovak Grant Agencies VEGA (Grant Nos. 1/0507/17 and 1/0712/18) and APVV (Grant No. APVV-17-0324) as well as from European Union's Horizon 2020 research and innovation program under the Marie Skłodowska-Curie Grant No. 752285. We acknowledge Dr Florian Chotard and Dr Alexander Romanov for a sample of (^{Ad}CAAC)AuCl.

Conflict of Interest

The authors declare no conflict of interest.

Supporting information

Supporting information (Materials and methods, synthesis and characterization, NMR spectra, DFT calculations, X Ray crystallography) can be found under: https://doi.org/xxxxx. CCDC 1972628-1972633 and CCDC 1984710 contain the crystallographic supporting information.

References.

[1] Selected reviews: a) H. Schmidbaur, A. Schier, *Arabian J. Sci. Eng.* **2012**, *37*, 1187-1225. b) A. S. K. Hashmi, G. J. Hutchings, *Angew. Chem. Int. Ed.* **2006**, *45*, 7896-7936. c) A. S. K. Hashmi, *Chem. Rev.* **2007**, *107*, 3180-3211. d) A. Fürstner, P. W. Davies, *Angew. Chem. Int. Ed.* **2007**, *46*, 3410 – 3449. e) S. Golunski, *Platinum Metals Rev*. **2013**, *57*, 82–84. f) M. Joost, A. Amgoune, D. Bourissou, *Angew. Chem. Int. Ed.* **2015**, *54*, 15022 – 15045. g) G. J. Hutchings, *ACS Cent. Sci.* **2018**, *4*, 1095-1101.

[2] a) P. Claus, *Appl. Catal. A-Gen.* **2005**, *291*, 222-229. b) L. McEwan, M. Julius, S. Roberts, J. C. Q. Fletcher, *Gold Bull*. **2010**, *43*, 298-306. c) M. Pan, A. J. Brush, Z. D. Pozun, H. Chul Ham, W.-Y. Yu, G. Henkelman, G. S. Hwang, C. B. Mullins, *Chem. Soc. Rev*. **2013**, *42*, 5002-5013. d) M. Pan, J. Gong, G. Dong, C. B. Mullins, *Acc. Chem. Res*. **2014**, *47*, 750-760. e) F. Cardenas-Lizana, M. A. Keane, *J. Mater. Sci*. **2013**, *48*, 543-564. f) M. A. Keane, M. Li, L. Collado, F. Cárdenas-Lizana, *Reac. Kinet. Mech. Cat.* **2018**, *125*, 25–36.

[3] Y. Ishikawa, Y. Yamamoto, N. Asao, *Catal. Sci. Technol.* **2013**, *3*, 2902-2905. (b) I. Saridakis, M. Kidonakis, M. Stratakis, *ChemCatChem* **2018**, *10*, 980 – 983. (c) H. Li, H. Guo, Z. Li, C. Wu, J. Li, C. Zhao, S. Guo, Y. Ding, W. He,Y. Li, *Chem. Sci*. **2018**, *9*, 4808–4813, and cited refs.

[4] a) P. Johnston, N. Carthey, G. J. Hutchings, *J. Am. Chem. Soc.* **2015**, *137*, 14548. b) G. Malta, S. A. Kondrat, S. J. Freakley, C. J. Davies, L. Lu, S. Dawson, A. Thetford, E. K. Gibson, D. J. Morgan, W. Jones, P. P. Wells, P. Johnston, C. R. A. Catlow, C. J. Kiely, G. J. Hutchings, *Science* **2017**, *355*, 1399–1403. c) G. Malta, S. J. Freakley, S. A. Kondrat, G. J. Hutchings, *Chem. Commun.* **2017**, *53*, 11733—11746. d) H. Xu, Hao, G. Luo, *J. Industr. Engin. Chem.* **2018**, *65*, 13-25.

[5] a) T. Bakarat, J. C. Rooke, E. Genty, R. Cousin, S. Siffert, B.-L. Su, *Energy Environment. Sci.* **2013**, *6*, 371, 391. b) J. A. Rodriguez, S. D. Senanayake, D. Stacchiola, P. Liu, J. Hrbek, *Acc. Chem. Res.* **2014**,

47, 773-782. c) M. Yang, S. Li, Y. Wang, J. A. Herron, Y. Xu, L. F. Allard, S. Lee, J. Huang, M. Mavrikakis, M. Flytzani- Stephanopoulos, *Science* **2014**, *346*, 1498–1501.

[6] a) N. Debono, M. Iglesias, F. Sanchez, *Adv. Synth. Catal.* **2007**, *349*, 2470–2476. b) H. Lv, J.-H. Zhan, Y.-B. Cai, Y. Yu, B. Wang, J.-L. Zhang, *J. Am. Chem. Soc*. **2012**, *134*, 16216-16227.

[7] Y. Satoh, M. Igarashi, K. Sato, S. Shimada, *ACS Catal.*, **2017**, *7*, 1836–1840.

[8] H. Ito, T. Saito, T. Miyahara, C. Zhong, M. Sawamura, *Organometallics* **2009**, *28*, 4829–4840.

[9] I. P. Silverwood, S. M. Rogers, S. K. Callear, S. F. Parker, C. R. A. Catlow, *Chem. Commun.* **2016**, *52*, 533–536.

[10] T. Whittaker, K. B. Sravan Kumar, C. Peterson, M. N. Pollock, L. C. Grabow, B. D. Chandler, *J. Am. Chem. Soc.* **2018**, *140*, 16469-16487.

[11] H. Li, H. Guo, Z. Li, C. Wu, J. Li, C. Zhao, S. Guo, Y. Ding, W. He, Y. Li, *Chem. Sci.* **2018**, *9*, 4808–4813

[12] a) E. Y. Tsui, P. Müller, J. P. Sadighi, *Angew. Chem. Int. Ed.* **2008**, *47*, 8937–8940; b) D. Gasperini, A. Collado, A. Gomez-Suarez,D. B. Cordes, A. M. Z. Slawin, S. P. Nolan, *Chem. Eur. J.* **2015**, *21*, 5403−5412.

[13] a) D. A. Rosca, D. A. Smith, D. L. Hughes, M. Bochmann, *Angew. Chem. Int. Ed.* **2012**, *51*, 10643–10646. b) A. Pintus, L. Rocchigiani, J. Fernandez–Cestau, P. H. M. Budzelaar, M. Bochmann, *Angew. Chem. Int. Ed.* **2016**, *55*, 12321–12324. c) L. Rocchigiani, J. Fernandez–Cestau, I. Chambrier, P. Hrobárik, M. Bochmann, *J. Am. Chem. Soc.* **2018**, *140*, 8287–8302. d) L. Rocchigiani, P. H. M. Budzelaar, M. Bochmann, *Chem. Sci.* **2019**, *10*, 2633–2642. e) G. Kleinhans, M. M. Hansmann, G. Guisado-Barrios, D. C. Liles, G. Bertrand, D. I. Bezuidenhout, *J. Am. Chem. Soc.* **2016**, *138*, 15873−15876.

[14] Reviews: a) A. J. Jordan, G. Lalic, J. P. Sadighi, *Chem. Rev*. **2016**, *116*, 8318−8372; b) H. Schmidbaur, H. G. Raubenheimer, L. Dobrzanska, *Chem. Soc. Rev.* **2014**, *43*, 345-380.

[15] For gold(III) complexes showing agostic CH bonding see F. Rekhroukh, L. Estévez, C. Bijani, K. Miqueu, A. Amgoune, D. Bourissou, *Angew. Chem. Int. Ed.* **2016**, *55*, 3414 –3418.

[16] a) X. Y. Liu, A. Wang, T. Zhang, C.-Y. Mou, *Nano Today* **2013**, *8*, 403-416. b) Y. Guo, R. Lang, B. Qiao, *Catalysts* **2019**, *9*, 135. c) L. Grinberga, J. Kleperis, G. Bajars, G. Vaivars, A. Lusis, *Solid State Ionics* **2008**, *179*, 42–45, and cited refs.

[17] D. Nabaho, J. W. Niemantsverdriet, M. Claeys, E. van Steen, *Catalysis Today* **2016**, *275*, 27–34.

[18] S. S. E. Collins, M. Cittadini, C. Pecharromàn, A. Martucci, P. Mulvaney, *ACS Nano* **201**5, *9*, 7846–7856.

[19] R. Guo, X. X. Xu, Y. Xia, W. Huang, Z. Li, B. Teng, *J. Catal.* **2018**, *368*, 379–388.

[20] P. Schlexer, G. Pacchioni, *J. Phys. Chem. C* **2017**, *121*, 14717−14724.

[21] J. Cornejo-Romeroa, A. Solis-Garcia, S. M. Vega-Diaz, J. C. Fierro-Gonzalez, *Mol. Catal.* **2017**, *433*, 391–402.

[22] N.-M. Zou, X.-C. Zhou, G.-Q. Chen, N. M. Andoy, W. Jung, G.-K. Liu, P. Chen, *Nat. Chem.* **2018**, *10*, 607–614.

[23] a) M. Green, A. G. Orpen, I. D. Salter, F. G. A. Stone, *J. Chem. Soc. Chem. Commun.* **1982**, 813-814. b) M. Green, A. G. Orpen, I. D. Salter, F. G. A. Stone, *J. Chem. Soc. Dalton Trans.* **1984**, 2497-2503.

[24] a) H. Lehner, D. Matt, P. S. Pregosin, L. M. Venanzi, A. Albinati, *J. Am. Chem. Soc.* **1982**, *104*, 6825-6827. b) A. Albinati, H. Lehner, L. M. Venanzi, M. Wolfer, *Inorg. Chem.* **1987**, *26*, 3933–3939.

[25] a) A. Antinolo, F. Carrillo, B. Chaudret, M. Fajardo, J. Fernandez-Baeza, M. Lanfranchi, H.-H. Limbach, M. Maurer, A. Otero, M. A. Pellinghelli, *Inorg. Chem.* **1994**, *33*, 5163–5164. b) A. Antinolo, F. Carrillo, B. Chaudret, M. Fajardo, J. Fernandez-Baeza, M. Lanfranchi, H.-H. Limbach, M. Maurer, A. Otero, M. A. Pellinghelli, *Inorg. Chem.* **1996**, *35*, 7873–7881.

[26] a) B. D. Alexander, B. J. Johnson, S. M. Johnson, P. D. Boyle, N. C. Kann, A. M. Mueting, L. H. Pignolet, *Inorg. Chem.* **1987**, *26*, 3506–3513; b) A. Albinati, L. M. Venanzi, G. Z. Wang, *Inorg. Chem*. **1993**, *32*, 3660-3669.

[27] B. D. Alexander, M. P. Gomez-Sal, P. R. Gannon, C. A. Blaine, P. D. Boyle, A. M. Mueting, L. H. Pignolet, *Inorg. Chem.* **1988**, *27*, 3301–3308.

[28] A. Hicken, A. J. P. White, M. R. Crimmin, *Angew. Chem. Int. Ed.* **2017**, *56*, 15127-15130.

[29] M. J. Butler, M. R. Crimmin, *Chem. Commun*. **2017**, *53*, 1348-1365.

[30] J. A. Martinho Simoes, J. L. Beauchamp, *Chem. Rev.* **1990**, *90*, 629–688.

[31] M. J. Butler, A. J. P. White, M. R. Crimmin, *Angew. Chem. Int. Ed*. **2016**, *55*, 6951–6953.

[32] J. W. Bruno, J. C. Huffman, K. G. Caulton, *J. Am. Chem. Soc.* **1984**, *106*, 444-445.

[33] H. Brunner, D. Mijolovic, *J. Organomet. Chem.* **1999**, *77*, 346-350.

[34] A. Albinati, R. Naegeli, A. Togni, L. M. Venanzi, *Organometallics* **1983**, *2*, 926-928

[35] T. Bauner, F. R. Wagner, R. Kempe, *Chem. Eur. J* **2013**, *19*, 8732-8735.

[36] a) L. F. Rhodes, J. C. Huffman, K. G. Caulton, *Inorg. Chim. Acta* **1992**, *198*, 639-649. b) H. Brunner, M. Muschiol, T. Neuhierl, B. Nuber, *Chem. Eur. J.* **1998**, *4*, 168-171. c) H. Brunner, D. Mijolovic, B. Wrackmeyer, B. Nuber, *J. Organomet. Chem.* **1999**, *579*, 298–303.

[37] a) D. F. Shriver, *J. Am. Chem. Soc*. **1963**, *85*, 3509-3510. b) X. Xu, Z. Sun, L.-P. Meng, S. Zheng, X. Y. Li, *Appl Organometal Chem*. **2019**, *33*, e4790.

[38] P. de Frémont, E. D. Stevens, M. R. Fructos, M. M. Diaz-Requejo, P. J. Pérez, S. P. Nolan, *Chem. Commun.* **2006**, 2045-2047

[39] A. S. K. Hashmi, C. Lothschütz, R Döpp, M. Rudolph, T. D. Ramamurthi, F. Rominger, *Angew. Chem. Int. Ed.* **2009**, *48*, 8243–8246.

[40] A. Romanov, M. Bochmann, *Organometallics* **2015**, *34*, 2439–2454.

[41] a) M. Rigoulet, S. Massou, E. D. S. Carrizo, S. Mallet-Ladeira, A. Amgoune, K. Miqueu, D. Bourissou, *PNAS* **2019**, *116*, 46-51. b) M. Straka, E. Andris, J. Vícha, A. Růžička, J. Roithová, L. Rulíšek, *Angew.*

Chem. Int. Ed. **2019**, *58*, 2011 –2016. c) J. Vícha, C. Foroutan-Nejad, M. Straka, *Nature Commun.* **2019**, *10*, 1643.

[42] I. Chambrier, D. L. Hughes, R. J. Jeans, A. J. Welch, P. H. M. Budzelaar, M. Bochmann, *Chem. Eur. J*, in press. http://dx.doi.org/10.1002/chem.201904790

[43] D.-A. Roşca, J. A. Wright, M. Bochmann, *Dalton Trans.* **2015**, *44*, 20785 – 20807.

[44] R. Kumar, C. Nevado, *Angew. Chem. Int. Ed.* **2017**, *56*, 1994 – 2015.

[45] L. Rocchigiani, J. Fernandez-Cestau, P. H. M. Budzelaar, M. Bochmann, *Chem. Commun.* **2017**, *53*, 4358, 4361.

[46] a) L. Rocchigiani, J. Fernandez-Cestau, Peter H. M. Budzelaar, M. Bochmann, *Chem. Eur. J.* **2018**, *24*, 8893 –8903. b) L. Currie, L. Rocchigiani, D. L. Hughes, M. Bochmann, *Dalton Trans*. **2018**, *47*, 6333-6343.

[47] I. Chambrier, L. Rocchigiani, D. L. Hughes, P. M. H. Budzelaar, M. Bochmann, *Chem. Eur. J.* **2018**, *24*, 11467 – 11474

[48] a) P. Pyykkö, *Angew. Chem. Int. Ed.* **2004**, *43*, 4412–4456; b) S. Alvarez, B. Menjón, A. Falceto, D. Casanova, P. Alemany, *Inorg. Chem.* **2014**, *53*, 12151−12163.